Grenoble, le 23 Aout 1977

CALCULATIONS AND MEASUREMENTS OF FAST NEUTRON SPECTRUM IN A RESEARCH REACTOR.

R. LLORET, R. PERDREAU, TRAN DAI Phuc.

Service des Piles
Centre d'Etudes Nucleaires de Grenoble
C E A FRANCE

2. Symposium on reactor dosimetry: dosimetry methods for fuels, cladding and structural materials.

CEA-CONF--4164

CALCULATIONS AND MEASUREMENTS OF FAST NEUTRON SPECTRUM IN A RESEARCH REACTOR.

R. LLORET, R. PERDREAU, TRAN DAI Phuc.

Service des Piles de Grenoble

Abstract :

. experimental program has been undertaken to confirm divers fast neutron spectrum calculations. The verification of calculational methods consists to compare measurements in a highly heterogenous media to two dimensional calculations effectuated on approach geometries.

The measurements have been carried out in two testing facilities located in the centre of the core and near the reflector of the MELUSINE Pool-type reactor.

Counting techniques used for the determination of the reaction rate by Beta-gamma activity measurements and activation foils are described. The following reactions have been selected : $^{197}Au(n,\gamma)\ ^{198}Au$, $^{115}In(n,n')\ ^{115}In_m$, $^{47}Ti(n,p)\ ^{47}Sc$, $^{58}Ni(n,p)\ ^{58}Fe$, $(n,p)\ ^{54}Mn$, $Ti(n,x)\ ^{46}Sc$, $^{56}Fe(n,p)\ ^{56}Mn$, $^{63}Cu(n,\alpha)\ ^{60}Co$, $^{27}Al(n,\alpha)\ ^{24}Na$, $^{92}Nb(n,2n)\ ^{92}Nb_m$, $^{58}Ni(n,2n)\ ^{57}Ni$.

A spectrum form has been elaborated from such activities by using the unfolding code SAND-II.

On other part, spectrum determinations are performed with transport computer codes ANISN and DOT-III. The spectrum obtained from Unfolding and Transport Codes have been compared.

Good agreement between the measured (foil activation) and calculated (SAND-II) activities were found with all detectors.

Reasonable agreement between transport (DOT-III) and iterative (SAND-II) solutions are observed in the two test cases.

This analysis permits to retain a spectrum determination procedure in the actual case of a composite testing facility.

CALCULS ET MESURES DE SPECTRES DE NEUTRONS RAPIDES DANS UN REACTEUR DE RECHERCHE.

R. LLORET, R. PERDREAU, TRAN DAI Phuc.

Service des Piles de Grenoble

RESUME

Un programme expérimental a été entrepris pour confirmer divers calculs de spectres de neutrons rapides.

Cette vérification de méthodes de calcul consiste à comparer des mesures en milieu fortement hétérogène aux calculs à deux dimensions menés sur des géométries approchantes.

Le mesure est effectuée dans deux éléments d'irradiation situés dans le coeur et près du réflecteur du réacteur piscine MELUSINE. On décrit les détecteurs par activation et les techniques de comptages utilisés, pour les réactions $^{197}Au(n,\gamma)\ ^{198}Au$, $^{115}In(n,n')\ ^{115}In_m$, $^{47}Ti(n,p)\ ^{47}Sc$, $^{58}Ni(n,p)\ ^{58}Co$, $^{54}Fe(n,p)\ ^{54}Mn$, $Ti(n,x)\ ^{46}Sc$, $^{56}Fe(n,p)\ ^{56}Mn$, $^{63}Cu(n,\alpha)\ ^{60}Co$, $^{27}Al(n,\alpha)\ ^{24}Na$, $^{92}Nb(n,2n)\ ^{92}Nb_m$, $^{58}Ni(n,2n)\ ^{57}Ni$.

Une forme de spectre est élaborée à partir de ces activités en utilisant la méthode de déconvolution SAND-II.

D'un côté, les calculs de spectre sont conduits au moyen des codes de transport ANISN et DOT 3. Les spectres obtenus par ces deux méthodes de calcul ont été comparés.

Une bonne concordance entre les activités mesurées (Méthode activation) et calculées (Méthode déconvolution) a été observée.

Une raisonnable concordance entre les spectres obtenus par les calculs de transport (DOT-III) et de déconvolution (SAND-II).

Cette analyse permet de retenir un procédé de détermination du spectre dans le cas concret d'un dispositif d'irradiation composite.

CALCULATIONS AND MEASUREMENTS OF FAST NEUTRON SPECTRUM IN A RESEARCH REACTOR

••••

I - INTRODUCTION

The development of several areas of reactor investigations such as integral reaction rates, radiation damage, dosimetry, isotope production, etc ..., is strongly dependent on the ability to determine accurately the neutron spectral distribution. Present calculation techniques which are used to obtain the spatial variation of the neutron spectr[illegible] using the S_n methods and the P-1 or P-3 approximation to s[illegible]he Boltzmann transport equation seem to be adequate f[illegible]ucing the neutron spectrum in a testing reactor. How[illegible]erent limitations exist when they are applied to [illegible]plex [illegible]ructure (heterogeneity) and to a large shield thickness. Fo[illegible] this reason, it is desirable to verify the accuracy and the approximations used in numerical techniques by measuring the neutron spectra at a specified location in a reactor system. Hence an experimental program has been carried out to provide test cases for neutron transport codes, to verify the input average neutron cross sections and the spatial variation of the calculated neutron spectrum. The measurements consist in irradiating several types of threshold detectors in two testing facilities, one located in the center of the core and the other near the reflector of the Melusine pool-type reactor. Activation rates are hence obtained for each type of considered foil and the data are the

TABLE I : Threshold detectors for fast spectrum determination

Reaction	T $1/_2$	Effective threshold energy (MeV)	E_γ (KeV)	I_γ (%)	References
$^{197}Au(n,\gamma)^{198}Au$	2.7 d	$4.9\ 10^{-6}$	0.412	95.45	1,4,6,7,8
$^{115}In(n,n')^{115m}In$	4.5 h	1.20	0.336	47.2	3,4,8
$^{47}Ti(n,p)^{47}Sc$	3.39 d	2.2	0.159	89.025	1,3,4,8
$^{58}Ni(n,p)^{58}Co$	70.78 d	2.8	0.811	99.44	2,4,8
$^{54}Fe(n,p)^{54}Mn$	312.6 d	3.1	0.835	99.97	2,3,4,8
$^{46}Ti(n,x)^{46}Sc$	83.85 d	3.9	0.889 1.121	99.984 99.987	1,2,3,4,8
$^{56}Fe(n,p)^{56}Mn$	2.576h	6.	0.847	99.	1,2,4,8
$^{63}Cu(n,\alpha)^{60}Co$	5.272y	6.8	1.173 1.332	99.86 99.906	2,3,4,8
$^{27}Al(n,\alpha)^{24}Na$	15.005h	7.2	1.369	99.993	1,3,4,8
$^{93}Nb(n,2n)^{92m}Nb$	10.16 d	10.234	0.934	99.	1,4,5,8
$^{58}Ni(n,2n)^{57}Ni$	36 h	13.5	1.370 0.511	86. 92.	1,3,4,8

h = hour
d = day
y = year

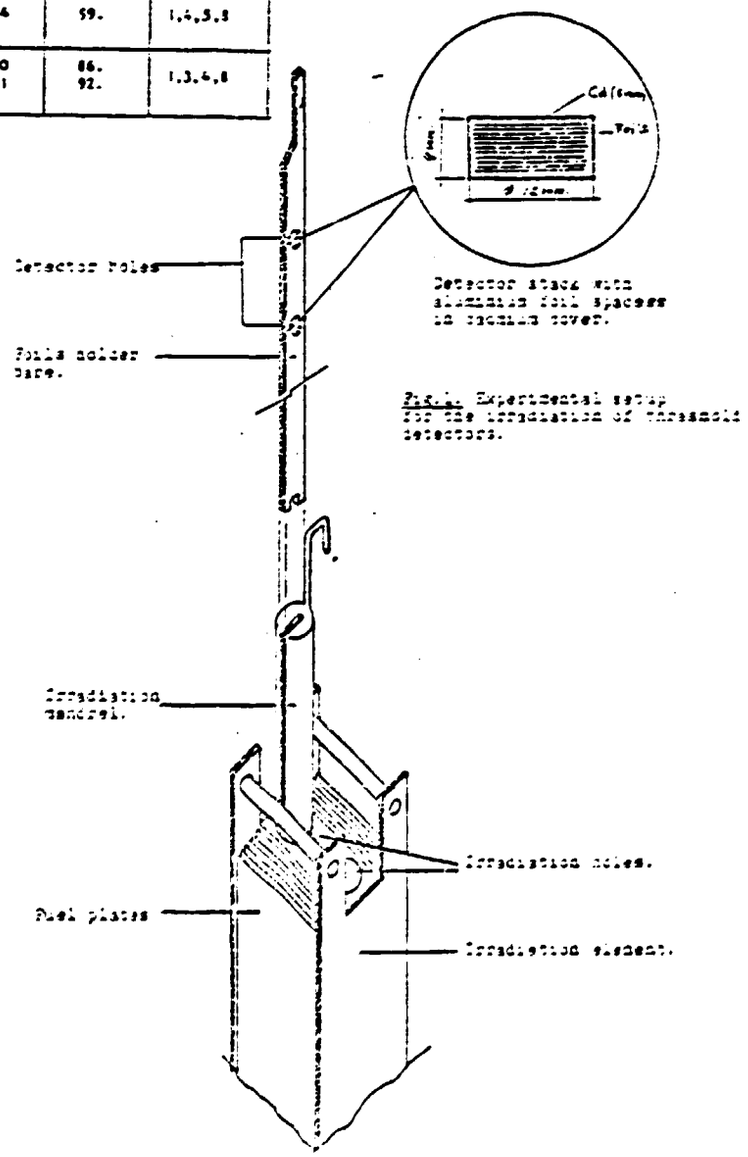

Detector stack with aluminium foil spacers in aluminium cover.

Fig.1. Experimental setup for the irradiation of threshold detectors.

transformed to energy spectrum by a multiple foil iterative code SAND II. This code is presented in part 2 of section II; section III deals with the transport calculation techniques; and comparison between calculated and measured results, discussion and remarks are given in section IV of this work.

II - EXPERIMENTAL METHOD

1. - Irradiation technique

The experimental set-up for the irradiations is shown in Fig.1. Each mandrel of the testing facility holds two sets of foils which are located at - 15 mm and - 50 mm from the median plane (maximum flux) of the reactor core. The monitors were in the form of 3 to 10 mm diameter and 0.1 to 1 mm thick samples, fabricated from 99.99 % pure natural metal, except for the resonance detector (197 Au) which is in the form of an alloy (Al-0.1 % Au) . The foils were irradiated in groups of 6 or8 and separated by aluminium foil spacers to prevent cross contamination. The stacks of foils were wrapped in a 0.6 mm thick cadmium cover to minimize the interfering activation reactions by thermal neutrons. Two irradiation compaigns have been undertaken, one for short half-life and the another for long half-life detectors, respectively one hour and 24 hours, in the reactor core with steady power level at 8 MW. The set of detectors utilized for determining the fast neutron spectrum, is given in Table 1 (1)to(8).

2. - Counting technique

Activation detectors are well suited to the problems of determining and comparing fast neutron energy distribution. In addition, the advantage of simplicity, small volume, low flux requirements and negligible gamma sensitivity, make them indispensable for the establishment of neutron spectra in nuclear reactors. The only limitation of such measurement is insufficient knowledge on energy dependence of the cross sectio

of some reactions in current use. When a material with a cross section, for a neutron reactor σ (E) is exposed in a neutron flux ϕ (E), the reaction rate per nucleus may be represented by the relation.

$$A = \int_0^\infty \sigma(E) \quad \phi \ (E) \ dE \qquad (1)$$

For spectrum monitoring, an ideal monitor is one for which the cross section as a function of energy is zero up to some threshold, at which it would rise abruptly to a precisely known constant value. Such step-function foils would provide an accurate measurement of the integrated flux above the threshold. Even with non-ideal detectors it is often useful to define average cross sections and effective thresholds when some knowledge of the spectrum is available. The quantities. are defined by

$$\int_0^\infty \sigma_i(E) \ \phi \ (E) \ dE = \bar{\sigma} \int_0^\infty \phi \ (E) \ dE = \sigma_{i_{eff}} \int_{E_{i.eff}}^\infty \phi(E) \ dE \qquad (2)$$

where $\bar{\sigma}$ is the average cross section, $\sigma_{i\text{-}eff}$ and $E_{i\text{-}eff}$ are the effective cross section and threshold energy of the i^{th} foil respectively.

After removal from the reactor and suitable cooling time, the gamma-ray activities of the irradiated samples were measured with a high resolution Ge(Li) detector of 50 cm3 volume. Samples were placed on a thin plexiglass hoder at a distance of 35 mm from the detector head. The Ge(Li) detector was well shielded by a 10 cm thick lead high volume enclosure. The absolute efficiency of the Ge(Li) detector for the detection of gamma-rays has been calibrated with ^{152}Eu multigamma standards and eight mono-energitic standards of activity, furnished by the LMRI* or calibrated in our laboratory by the coincidence technique. The pulse height spectrum is recorded by the Plurimat analyser

---

* Laboratoire de Metrologie des Rayonnements Ionisants. Commissariat à l'Energie Atomique - CEN - SACLAY

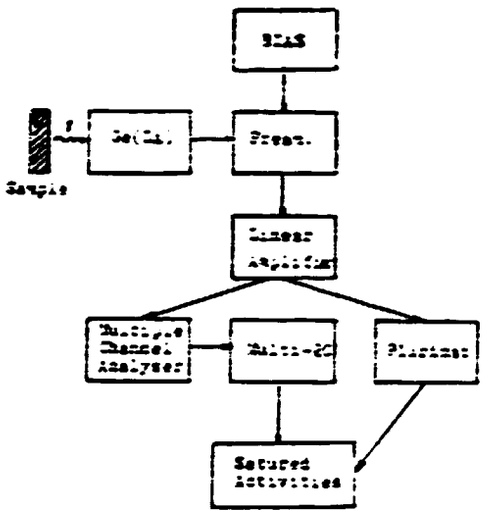

Fig. 2. Block diagram of the experimental setup for gamma counting.

(Intertechnique). The Block-diagram of the experimental set-up for gamma counting is given in Fig.2. Corrections are applied to the measurements to account for the flux disturbance due to the foils during irradiation and self-absorption of the gammas during the counting period. Both of these effects are estimated to be very small due to the small dimensions of the detectors.

The photopeak counts were analysed and converted numerically by the Multi-20 computer to disintegration rates suitable for input to the spectrum determining code SAND-II (9) (spectrum Analysis by Neutron Detectors) by a numerical program which takes into account, isotopic abundancies, atomic weight, counter efficiency, decay constant, irradiation time, cooling time, counting time and gamma branching ratios of each foil, as inputs. The results of this computation give the saturated activity is disintegrations per second (Becquerel) per nucleus; accuracy of such measurements is within 1.5 to 3 % (1σ).

3. - Spectrum derived from measurements

The shapes and amplitudes of the spectra were then determined by the unfolding computer code SAND-II which proceeds from a trial flux (obtained from transport calculations developed in section III) to an iterative flux solution. From the trial flux, the iteration procedure to a solution flux spectrum may be summarized as follows; it is described in detail in reference (9).

The calculated activity for the i^{th} foil induced by neutrons in the j^{th} energy interval (between E_j and E_{j+1}) based on the k^{th} iteration is given by the relationship.

$$A_{i,j}^{k} = \int_{E_j}^{E_{j+1}} \sigma_i (E)\, \phi^{k} (E)\, dE \qquad (3)$$

SAND-II assumes the integral in equation (3) may be approximated by

$$A_{i,j}^{k} = \bar{\sigma}_{i,j}\, \phi_j^{k} \qquad (4)$$

where $$\phi_j^k = \int_{E_j}^{E_{j+1}} \phi^k (E)\, dE \qquad (5)$$

and $$\bar{\sigma}_{i,j} = \frac{\int_j^{E_{j+1}} \sigma_i (E)\, dE}{\int_{E_j}^{E_{j+1}} dE} \qquad (6)$$

are the CSTAPE (auxillary program of SAND-II) average cross section and are independent of k, and do not, therefore, require recalculation at each iteration.

The iteration proceeds by introducing an activity weighting function.

$$W_{i,j}^k = 1/2 \left(A_{i,j}^k + A_{i,j-1}^k\right) \Big/ A_i^k \qquad (7)$$

i = foil index
j = energy interval index (2...620)
k = iteration index

For the i^{th} foil

$$A_i^k = \sum_{j=1}^{620} A_{i,j}^k \qquad (8)$$

is the total calculated activity of the i^{th} detector at the k^{th} iteration. $W_{i,j}^k$ represents the importance of interaction with neutrons in the j^{th} energy group to the total activity of the i^{th} foil. The ratio of measured to calculated activity fc. the i^{th} monitor at the k^{th} iteration is defined as

$$R_i^k \equiv Ai \; / \; A_i^k \qquad (9)$$

Finally C_j^k is defined by

$$\ln C_j^k = \left(\sum_{i=1}^{n} W_{i,j}^k \ln R_i^k\right) \Big/ \left(\sum_{i=1}^{n} W_{i,j}^k\right) \qquad (10)$$

5.

FOIL REACTION	SATURATED MEASURED ACTIVITY (DPS/NUCLEUS)	SATURATED CALCULATED ACTIVITY (DPS/NUCLEUS)	NOMINAL * 9.?? PERCENT ACTIVITY LIMITS (MEV)		RATIO MEASURED TO CALCULATED ACTIVITIES
			LOWER	UPPER	
AU197(N,G)AU198 CD	1.833E-09	1.733E-10	4.384E-06	7.684E-05	1.0549
IN115(N,N')IN115M	1.291E-11	1.369E-11	1.123E 00	5.790E 00	0.9435
TI47(N,P)SC47	1.159E-12	1.194E-12	2.139E 00	6.447E 00	0.9714
NI58(N,P)CO58	7.210E-12	7.226E-12	2.139E 00	7.524E 00	1.3241
FE54(N,P)MN54	5.194E-12	4.167E-12	2.294E 00	7.930E 00	0.9937
TI46(N,P)SC46	7.935E-13	7.574E-13	3.404E 00	8.235E 00	0.9045
FE56(N,P)MN56	7.641E-14	7.433E-14	5.534E 00	1.130E 01	1.3311
CU63(N,A)CO60	3.276E-14	3.247E-14	5.544E 00	1.129E 01	1.3179
AL27(N,A)NA24	6.513E-14	6.540E-14	6.434E 00	1.223E 01	1.9422
[illegible](N,2N)[illegible]	2.767E-16	2.784E-16	9.934E 00	1.443E 01	1.3053
NI58(N,2N)NI57	2.358E-16	2.354E-16	1.383E 01	1.723E 01	1.3031

* The energy limits within which 90 % of activity is produced.

Table 2. SAND-II Solution results obtained after 8 iterations for the 44 G location.

FOIL REACTION	SATURATED MEASURED ACTIVITY (DPS/NUCLEUS)	SATURATED CALCULATED ACTIVITY (DPS/NUCLEUS)	NOMINAL * 9.?? PERCENT ACTIVITY LIMITS (MEV)		RATIO MEASURED TO CALCULATED ACTIVITIES
			LOWER	UPPER	
AU197(N,G)AU198 CD	[illegible]	[illegible]	4.23?E-0?	7.2??E-05	[illegible]
IN115(N,N')IN115M	[illegible]	[illegible]	[illegible]	5.7??E 00	[illegible]
TI47(N,P)SC47	4.8??E-13	4.833E-13	2.1??E 00	6.4??E 00	1.0442
NI58(N,P)CO58	5.1??E-12	5.21?E-12	2.1??E 00	7.5??E 00	1.12?3
FE54(N,P)MN54	3.84?E-12	3.?4?E-12	2.2??E 00	7.9??E 00	[illegible]
TI46(N,P)SC46	5.8??E-13	5.4??E-13	3.4??E 00	8.2??E 00	[illegible]
FE56(N,P)MN56	5.3??E-14	5.??9E-14	5.5??E 00	1.1??E 01	[illegible]
CU63(N,A)CO60	2.4??E-14	2.3??E-14	3.4??E 00	1.12?E 01	1.1155
AL27(N,A)NA24	3.3??E-14	3.3??E-14	4.4??E 00	1.23?E 01	1.0449
[illegible](N,2N)[illegible]	2.?3?E-16	2.34?E-16	[illegible]	[illegible]	[illegible]
NI58(N,2N)NI57	[illegible]	[illegible]	[illegible]	1.72?E 01	[illegible]

* The energy limits within which 90 % of activity is produced.

Table 3. SAND-II Solution results obtained after 0 iterations for the 46 G location.

which is the correction factor to be assigned to the next iteration. It is affected most by those foils where the reaction rate with neutrons in energy group j is largest. From C_j^k and ϕ_j^k the next flux is hence computed according to

$$\phi_j^{k+1} = \phi_j^k \; C_j^k \qquad (11)$$

for all j's such that $\sum_{i=1}^{n} W_{i,j}^k \neq 0$.

For all j's such that $\sum_{i=1}^{n} W_{i,j}^k = 0$ (which means there is a region in which none of the cross section is sensitive), the next k + 1 value of the differential flux is interpolated from neighboring regions (the nearest lower j and the nearest higher j for which $\sum_{i=1}^{n} W_{i,j}^k \neq 0$). Moreover, if such an insensitive region occurs at either extreme space, extrapolation is then performed (below or above, as required) by SAND-II according to one of several alternate and classical forms specified by the user.

Iterations are repeated until standard deviation of the calculated activities from the measured activities is less than a percentage specified by the user, or until the change in the standard deviation of activities from one iteration to the next is less than 1 %, or until a specified number of iterations has been reached.

The measured and calculated (by unfolding code) activities are given in Tables 2 and 3.

III - CALCULATION METHODS

The irradiation of reactor structural materials are often performed in test reactors with special testing facilities. The purpose of these facilities is to represent physically and chemically (temperature, moderator, nature and intensity of nuclear radiation, etc ...) as well as possible the anticipated

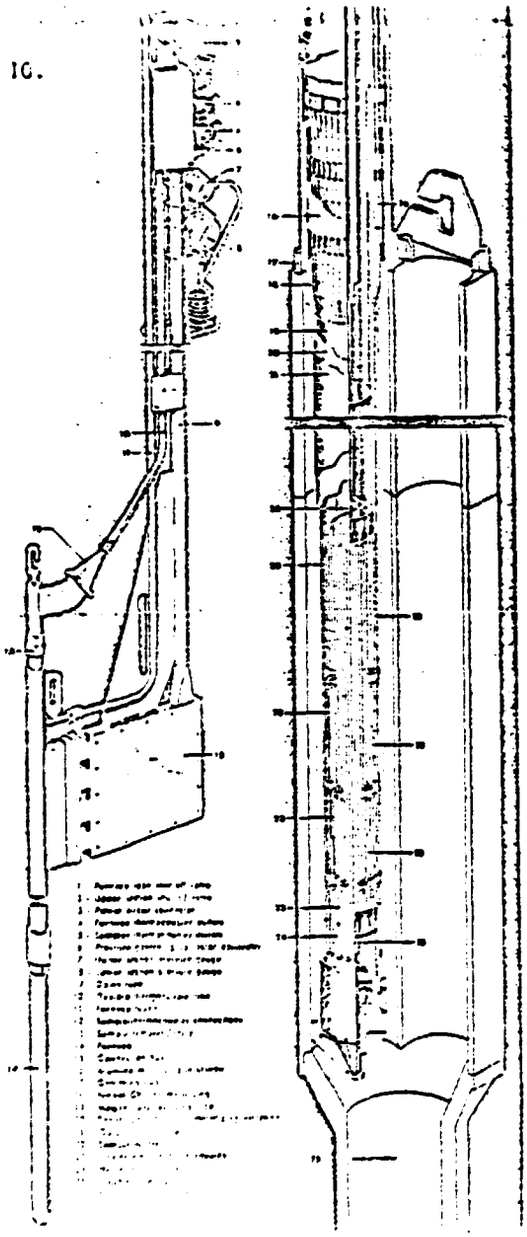

Fig. 1 : The complexe structure (secure (Heterogeneity) of the Chooz rig.

DESCRIPTION

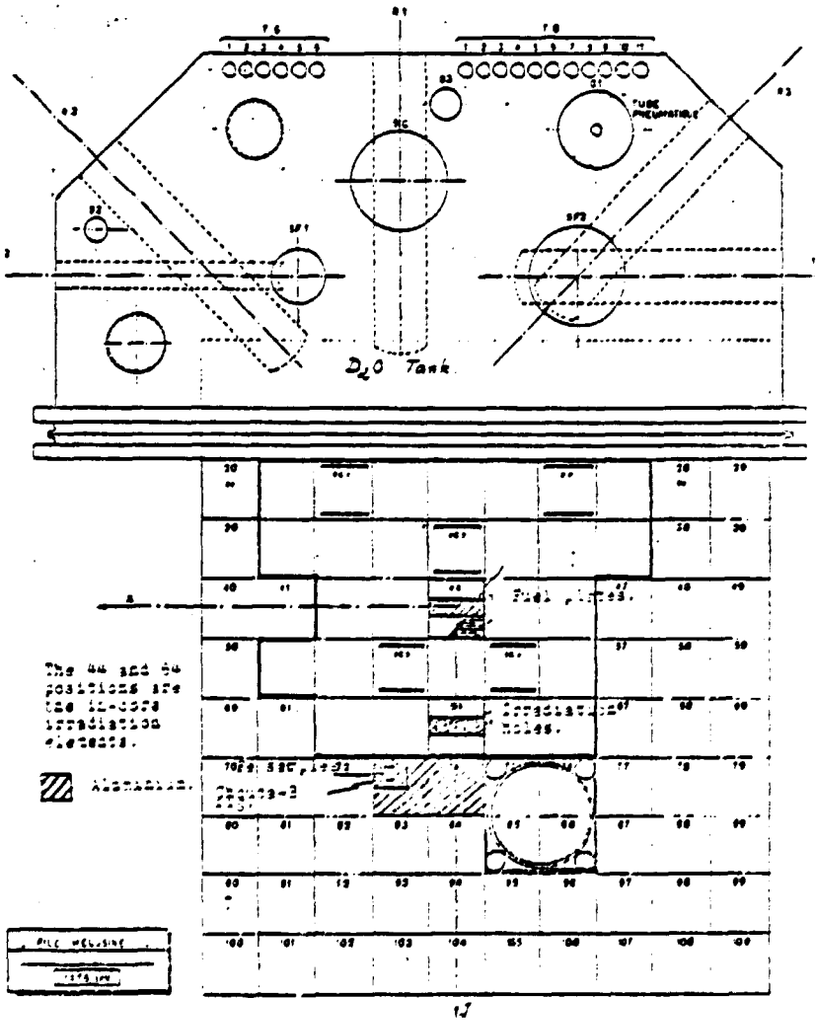

Fig. : Cross-sectional view of the core and surroundings of the reducing reactor.

working conditions of such materials in a nuclear power reactor. Such apparatus form highly heterogeneous media with regard to the radiation source of the reactor, as shown in figure 3 with the complex structure feature of the testing rig Chouca B used in Melusine.

Under these circumstances, the accurate determination of the neutron flux distribution within reactor lattices is often difficult for the two following reasons : firstly, reasonably high order angular approximations are required to determine the detailed flux variations within lattice cells, and secondly because reactors tend to be large in terms of the numbers of both lattice cells and mean-free-paths. So many spatial coarse mesh intervals are required to represent the lattice structure accurately and to reduce truncation errors to an acceptable level. The finite element method is more suitable to treat such problems but unfortunately a transport code using the finite element model is not yet available. Hence multigroup discrete ordinates transport codes ANISN and DOT-III have been adopted to reproduce the neutron spatial distribution in the two irradiation locations in the Melusine reactor.

1. - Calculation procedure

For the fast neutron spectrum analysis, the transport discrete ordinates (S_n) method can give a good representation of neutron flow near boundaries and other locations of the reactor where the flux is rapidly varying, because the angular dependence of the flux is explicitly determined, in spite of some ray-effects observed in such a method.

Calculations have been performed for the two special irradiation locations (44G and 64G) in the reactor core (Fig.4) in the following manner :

a) 100 energy group cross-sections are derived from ENDF/B-III nuclear data file.

b) Cross-sections and neutron physical constants of homogenized cells are obtained by reducing into 26 suitable energy groups

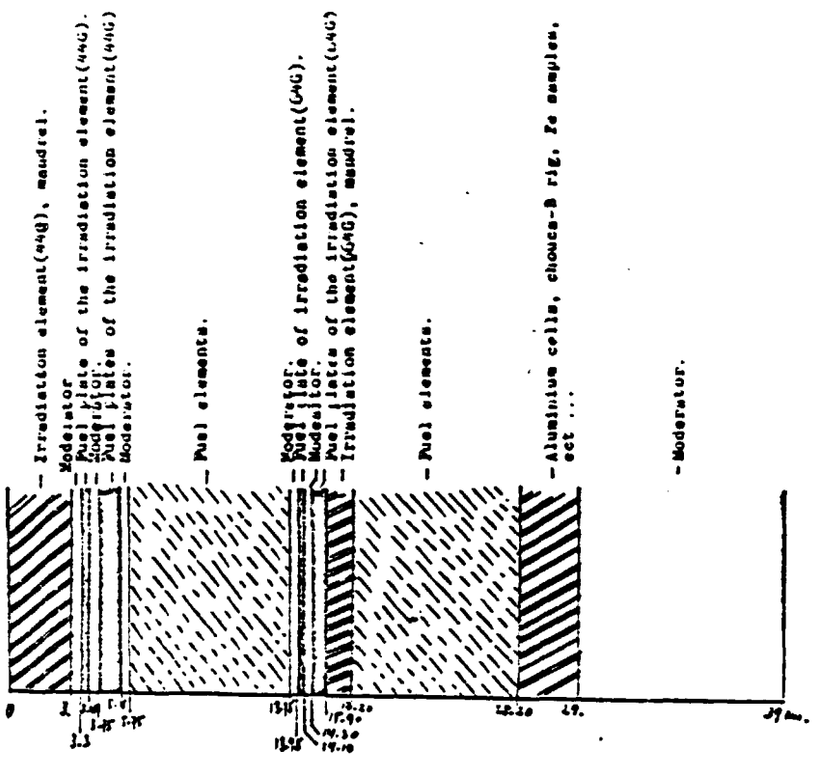

Fig.5. Cylindrycal cell homogenisation of the MELUSINE reactor Core and Environment, used in the One-Dimensional Trans,ort Code ANISN.

Fig.6. The(X-Y) cylindrical model of the MELUSINE reactor,used in the Two-Dimensional Trans,ort Code DOT-III calculation; the numberof mesh intervals I(X) are in the marks, all difensions are in centimeters.

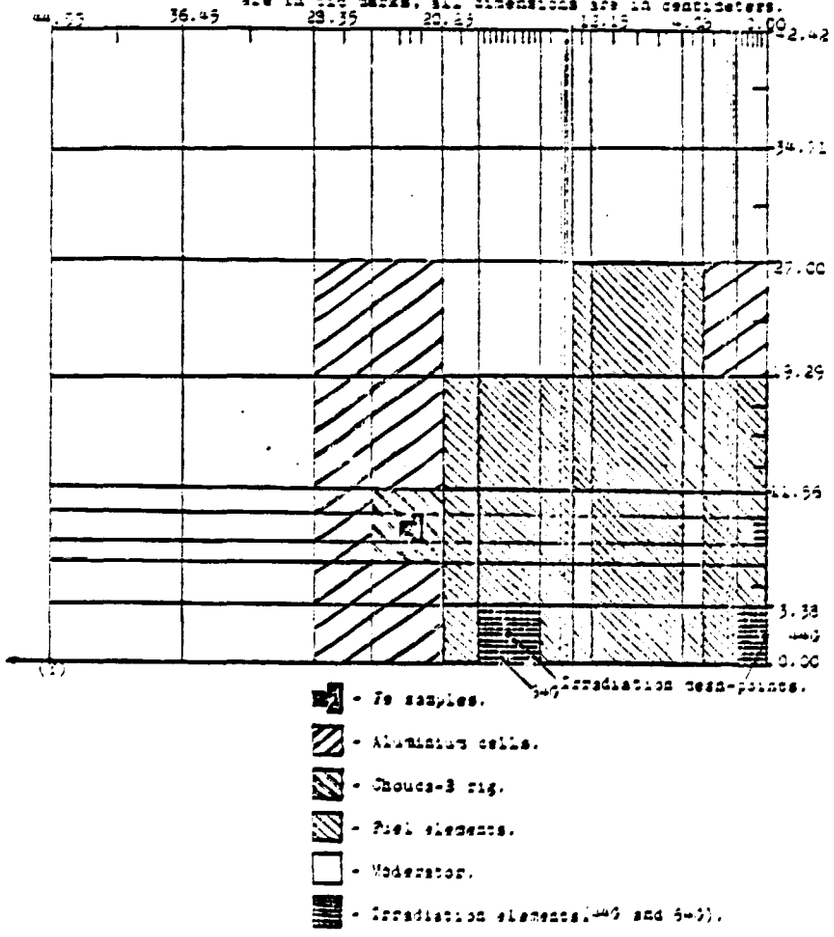

(with reasonable short lethargy intervals to reduce errors caused by averaging the constant over the interval) the 100 energy groups spectrum by the one-dimensional transport code ANISN (10),(11) (Discrete Ordinate Transport with Anisotropic Scattering).

The typical reactor core consists of discrete local regions of fuel, moderator, coolant, control rods and structural materials all homogenized and arranged in a "semi-regular" cylindrical geometry; as shown in figure 5; global flux distribution is obtained from transport approximation S_6/P_3. Fuel, water and structural materials are assumed to be homogenized over the volume of the unit cell,and the characteristics of the cell (e.g. densities of nuclei, % Burn-up etc ...) are computed for the homogeneous mixture, and are distributed in concentric cylindrical layers. A suitable energy-distribution fission source has been considered in the calculation.

c) The core cross-section as a cylinder based on the (x,y) model is considered in the two-dimensional transport code DOT-III (12), (13) using the homogenized cross sections and physical constants from part b); the reaction rates and the spatial flux distribution are determined with S_{12}/P_3 approximation for the two test cases.

Simplifying assumptions to make a mathematically tractable physical model for the reactor structural features (heterogeneity) are required; and in order to reduce the computer memory and the time in the C.P.U., a hypothetical symmetrical geometry assumption is made, as represented in Fig.6. Thus the exact reactor power level distribution could not be correctly reproduced. In spite of such simplification, up to 28 radial and 45 axial fine-mesh intervals are required. They represent about 1260 calculated mesh-points.Since the important problem associated with homogenization is the difference in flux levels in different materials within the cell, the region of interest should be at least one diffusion length from a material interface source discontinuity, so 10 fine-mesh intervals are used in the(44G and 64G) coarse-mesh cells considered.

FLUX / UNIT LETHARGY.
10.130
1.0Y
11.310
100.0Y
MeV/F.ECH.
0.000
10.0EV
4.000
100.0EV
0.203
1.0EV
0.000
10.0EV
-0.103
10.0EV

FLUX / UNIT LETHARGY.
10.130
1.0Y
11.310
100.0Y
MeV/F.ECH.
0.000
10.0EV
4.000
100.0EV
0.203
1.0EV
0.000
10.0EV
-0.103
10.0EV

Suitable radial and axial power distribution throughout the core have been considered. Energy group discretization has been chosen to represent adequately the energy domain of interest (0.1 to 10 MeV) and for the considered threshold detector cross—sections.

The results of calculated differential neutron energy dependence spectra are plotted in Fig.7 and 8.

IV - RESULTS AND DISCUSSION

The comparison of differential flux spectrum between unfolding and transport calculations are represented in Fig.9 and 10, for the two irradiation locations.

The solid curve is the theoretically calculated input spectrum and the dashed curve is the iterative solution. A close similarity between the expected (DOT-III) and the SAND-II solutions is observed in the limited energy region between 0.1 MeV and 10 MeV, even though individual experimental uncertainties exist with respect to activities and accurate knowledge of cross-section data.

The differential flux comparison given in Fig.9 and 10. Shows rather substantial disagreement between the theoretical and the SAND-2 solutions over certain energy limits, for both test cases (44G and 64G), notably from 0.1 to 1 MeV where errors are within $\pm$ 10 % (error already present due to the inaccuracy of the cross-sections !).

The results have been arbitrarily normalized at the energy over 1 MeV (as stated in Part c, paragraph 1 of section 2 due to simplifying assumptions in reactor geometry; the real reactor power level is therefore not correctly reproduced by the transport codes). Such normalization does not necessarily optimize the comparison for all neutron energies. The ratios of differential flux of transport and unfolding calculations

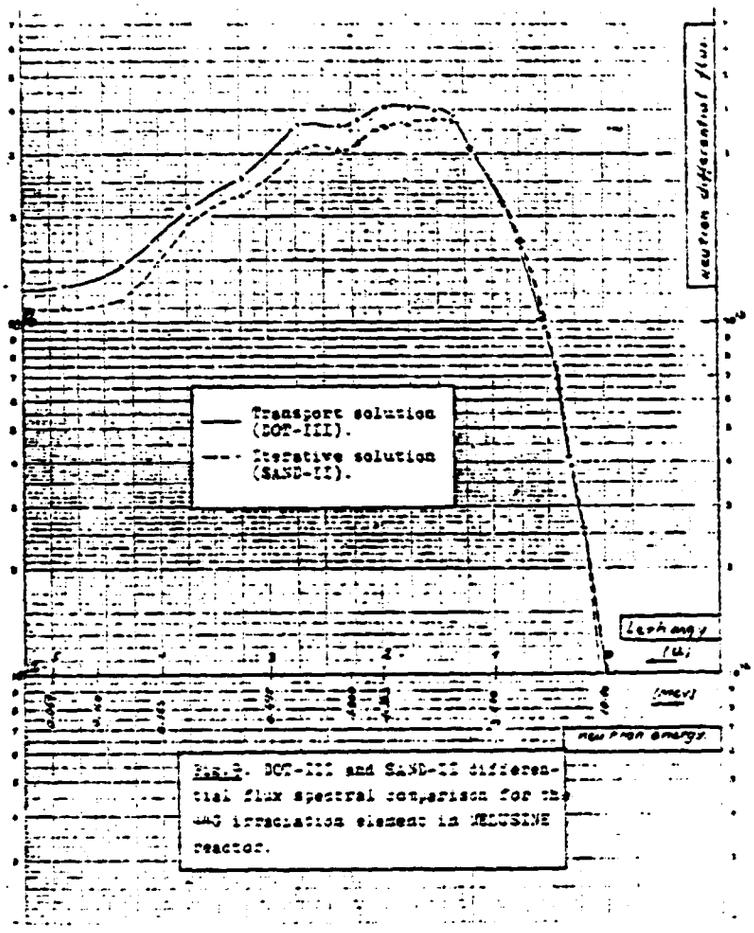

Fig. 9. DOT-III and SAND-II differential flux spectral comparison for the 4MG irradiation element in MELUSINE reactor.

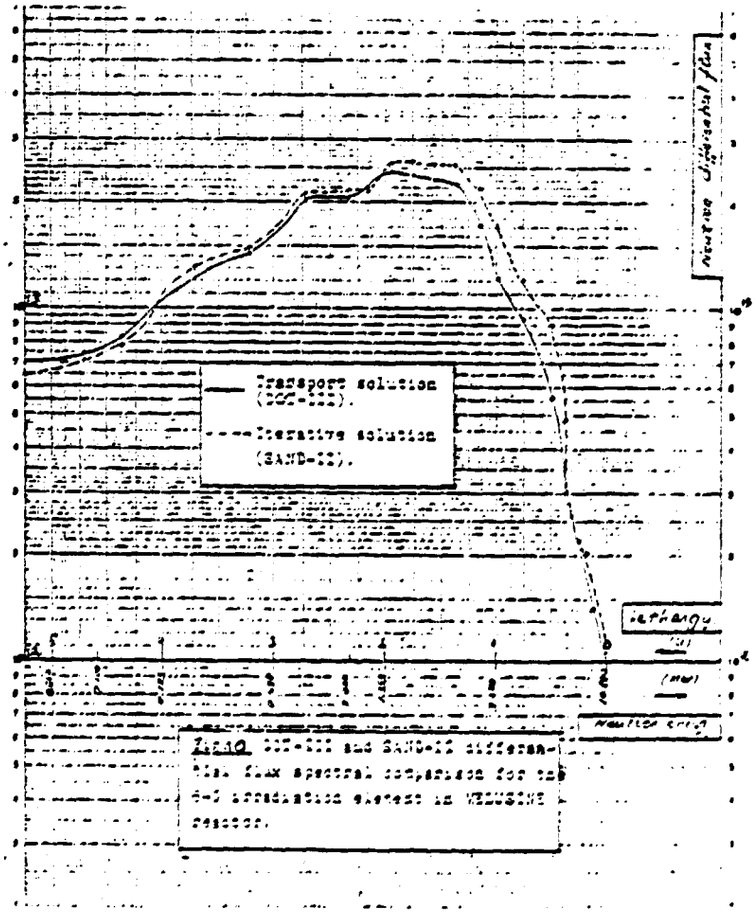

Fig. 10. DOT-III and SAND-II differential flux spectral comparison for the 6-J irradiation element in MELUSINE reactor.

with a normalization factor ρ ($\rho = \frac{\phi \text{ DOT-III}}{\phi_{>1} \text{ DOT-III}} \Big/ \frac{\phi \text{ SAND-II}}{\phi_{>1} \text{ SAND-II}}$)
are given in Tables 4 and 5, and represented in Fig.11 and 12 for the 44G and 64G irradiation locations, respectively. The large deviation ± 15 % observed from 0.067 to 1 MeV may be due to the insufficient number of foils with overlapping energy in that region, and the utilization of the single resonant detector 197 Au (with most of its sensitivity outside the well covered energy region) may have introduced additional errors.

The accuracy to which the spectrum are known can be estimated from percent deviations of measured and calculated activities given in Tables 2 and 3. The deviations vary from less than 1 % to about 3 % for various reactions utilized in the two considered spectrum. The sign of the deviation from those foils with numerically large deviation is consistently positive or negative, suggesting that there is considerable uncertainty in the knowledge of the normalization of some of the activation cross sections, as stated in studies made by Vlasov (14), McElroy W.N. and Kellog (15), Fabry (16), Grundl (17), Zijp (18), Paulsen (19), SimonsR.L. and McELROY W.N.(20) and many others; and also that the integrated accuracy of present evaluated cross sections is within ± 10 %, depending on the energy region, for a great number of foil detector reactions in current use. It is concluded that quasi every trial spectrum fits the measured activation data and represents correctly the real irradiation locations under consideration.

V - CONCLUSION

In spite of the difficulties arising in interpreting the experimental results, it should be emphasized that part of the uncertainties are due to the inherent non-uniqueness of the solution of the type of integral equations, to the inaccurate knowledge in available cross section data and to the measured values of saturated activities, and the simplifying assumptions

Neutron Energy (MeV)	Differential Neutron flux: Calculated initial spectrum DOT III	Differential Neutron flux: Iterative solution SAND-II	$\beta = \frac{\phi\ DOT}{\phi\ SAND} = \frac{\phi_{>1MeV}^{SAND}}{\phi_{>1MeV}^{DOT}}$
	$\phi_{>1MeV} = 3.361 \times 10^{13}$	$\phi_{>1MeV} = 3.170 \times 10^{13}$	
.1025	1.385×10^{13}	1.128×10^{13}	1.08
0.123	1.421×10^{13}	1.179×10^{13}	1.12
0.235	2.102×10^{13}	1.877×10^{13}	1.17
0.388	2.300×10^{13}	2.166×10^{13}	1.08
.639	3.566×10^{13}	3.164×10^{13}	1.12
.908	3.314×10^{13}	2.934×10^{13}	1.11
1.050	3.737×10^{13}	3.057×10^{13}	1.14
1.350	4.027×10^{13}	3.451×10^{13}	1.08
1.630	3.994×10^{13}	3.329×10^{13}	1.05
2.350	3.863×10^{13}	3.536×10^{13}	1.01
2.450	3.810×10^{13}	3.589×10^{13}	0.99
3.050	3.018×10^{13}	2.940×10^{13}	0.95
3.650	2.085×10^{13}	2.148×10^{13}	0.90
4.450	1.387×10^{13}	1.673×10^{13}	0.88
5.450	9.607×10^{12}	1.067×10^{13}	0.85
6.350	5.869×10^{12}	6.674×10^{12}	0.82
7.050	3.786×10^{12}	4.282×10^{12}	0.83
7.750	2.404×10^{12}	2.785×10^{12}	0.80
10.500	7.881×10^{11}	8.416×10^{11}	1.16

TABLE 4 : DOT III - SAND-II (after 8th iteration) differential neutron flux comparison for the 44 C location.

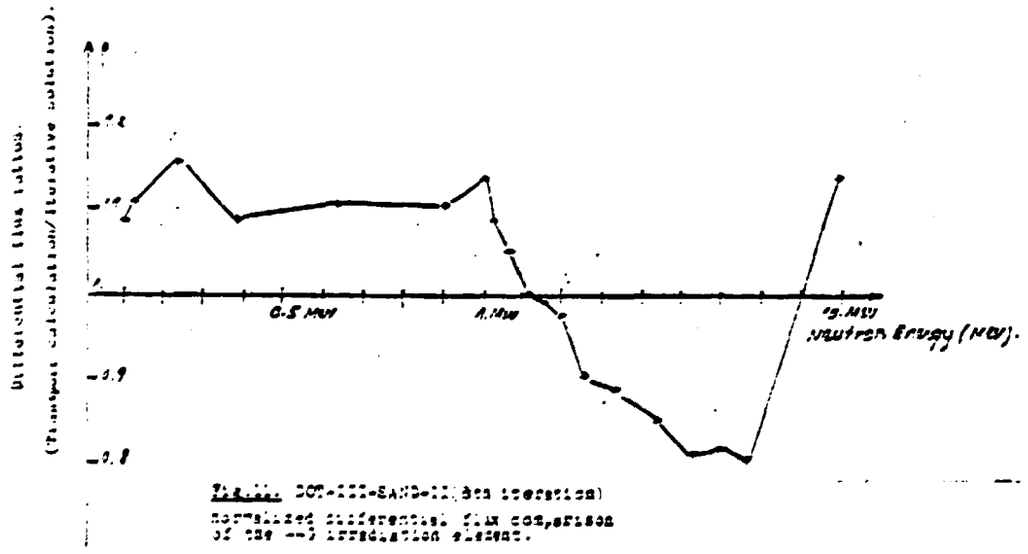

Fig. 4.4 DOT-III-SAND-II (8th iteration)
Normalized differential flux spectra at the end of the irradiation element.

to make a mathematically tractable physical model used in the transport code represent quite well the real condition of the experiment developed above in this work. The multiple foil iterative method, apart from determining neutron flux spectra, could be used as an adjunctive test to the reactor physics calculationnal methods; even though the iterative solution obtained by SAND-II is not unique. The method should give energy-dependent differential neutron flux results with accuracies $\pm$ 10 % depending on experimental conditions. Within adequate foil coverage, differential flux spectra reflect roughly the true structure but can introduce fluctuation resulting errors in foil reaction cross sections or measured activities; as expected in Fig.9 and 10, the solution are more tightly defined in the central energy region considered than at the ends where fewer aetivities on thresholds occur.

The use of a large number of foils with overlapping energy regions of sensitivity (especially from 0.5 to 3 MeV in our case : radiation damage studies) and subsequent analysis of the iterative and transport solutions of the differential flux spectrum may help distinguish the true spectrum from that caused by errors in cross section, in activity measurements and from foil stack self-absorption scattering. A simple foil with most of its sensitivity outside the well overlapped energy region is not recommended, due to its additional errors.

NEUTRON ENERGY (MeV)	differential Neutron flux		$\frac{\phi \text{ DOT}}{\phi \text{ SAND}}$ or $\frac{\phi_{>1}(\text{SAND})}{\phi_{>1}(\text{DOT})}$
	Calculated trial Spectrum DOT III	Iterative solution SAND-II	
	$\phi = 1.235 \times 10^{13}$ $\phi_{>.1\text{MeV}}$	$\phi = 1.844 \times 10^{13}$ $\phi_{>.1\text{MeV}}$	
.102	7.405×10^{12}	7.336×10^{12}	1.16
.123	8.065×10^{12}	7.976×10^{12}	1.20
.235	1.289×10^{13}	1.338×10^{13}	1.07
.388	1.448×10^{13}	1.383×10^{13}	1.08
.639	2.070×10^{13}	2.132×10^{13}	1.14
.900	2.038×10^{13}	2.146×10^{13}	1.12
1.050	2.179×10^{13}	2.244×10^{13}	1.13
1.350	2.347×10^{13}	2.337×10^{13}	1.09
1.650	2.332×10^{13}	2.425×10^{13}	1.05
2.050	2.244×10^{13}	2.640×10^{13}	1.00
2.450	2.215×10^{13}	2.678×10^{13}	0.98
3.053	1.746×10^{13}	2.206×10^{13}	0.94
3.650	1.208×10^{13}	1.611×10^{13}	0.89
4.450	9.194×10^{12}	1.234×10^{13}	0.87
5.450	5.566×10^{12}	7.679×10^{12}	0.86
6.350	3.462×10^{12}	4.818×10^{12}	0.84
7.250	2.193×10^{12}	3.078×10^{12}	0.84
7.750	1.194×10^{12}	2.010×10^{12}	0.82
10.50	4.581×10^{11}	4.331×10^{11}	1.19

TABLE 5. DOT III - SAND-II (after 7th iteration) differential neutron flux comparison for the 4-3 location.

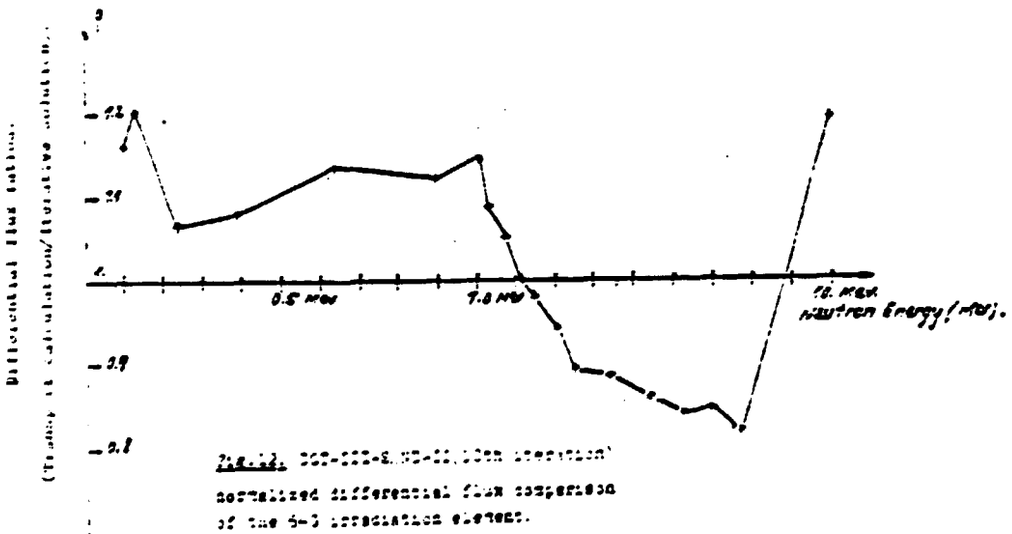

Fig. 12. DOT-III-SAND-II (7th iteration) normalized differential flux comparison of the 4-3 irradiation position.

REFERENCES

1. LEDERER. Table des Isotopes, John-Wiley Ed.

2. LMRI, Table Radionucléides 1975, Saclay.

3. HELMER R.G. et GREENWOOD R.C." Evaluated Decay Scheme Data" Nuclear Tech. V.25,2/75.

4. FABRY A. "Review of microscopic integral cross-section data in fundamental reactor dosimetry Benchmarck neutron fiels" AIEA, Vienne 10/76.

5. TENNENT R.M" Science data book" Oliver et Boyd Ed.

6. HELISTRAND Eric : "Reactor physics in the resonance and thermal regions", V II, MIT press. 1966, p. 151-173.

7. EDWARD PROFIO A."Experimental Reactor Physics" John Wiley editor 1976.

8. divers : Nuclear data sheets.
   Hanbook of Chemistry and Physics. 57th Ed. 1976-77

9. Mc ELROY W.N. and BERG S. "A computer-Automated Iterative Method for Neutron Flux Spectra Determination by Foil Activations" AFWL-TR 67-41 Vol I, II, IV.

10. ENGLE W.W. Jr., "A User's Manual for ANISN, A one Dimensional Discrete Ordinates Transport Code with Anisotropic Scattering," K-1693, Oak-Ridge National Laboratory (1973).

11. DEVILLERS C. "Système ANISN. Description et Mode d'utilisation du programme aux ordonnées discrètes ANISN et des programmes auxilliaires" C.E.A.-N-1358 (1970).

12. MYMATT F.R. et al, "The DOT-III Two-Dimensional ordinate Transport Code", ORNL-TM-4280, Oak-Ridge National Laboratory (1973).

13. BRANDICOURT A. et al, "Mode d'utilisation du Programme de Transport aux ordonnées discrètes à deux dimensions DOT-III". Rapport SERMA/Saclay n° 224-1/76.

14. VLASOV M., DUNFORD C., SCHMIDT J.J., and LEMMEL H.D., "Status of Neutron Cross section Data for Reactor Radiation Measurements", INDC (NDS) 47/L, IAEA, Vienna (1972).

15. Mc ELROY W.N. and KELLOGG S. "Fuel and Materials Fast-reactor Dosimetry Data developpement and Testing" Nucl. Techn. V.25 n° 2 p. 169-223 (2/1975).

16. FABRY A., "Evaluation of Microscopic Cross-sections averaged in the Uranium-235 Thermal Fission Neutron Spectrum (for 29 Nuclear Reactions Relevant to Neutron Dosimetry and Fast Reaction Technology) BLG-465, Centre d'Etudes de l'Energie Nucléaire, Mol, Belgium (1972).

17. GRUNDL J.A., and HANSEN G.E. "Measurement of Average Cross-section Ratios in fundamental Fast-neutron Spectra", in Nuclear Data for Reactor Vol.I, pp 321-336, IAEA, Vienna (1967).

./...

18. ZIJP W.L., VOORSRAAK W.P. and SOLTHEXIUS H.J., "Compilation of Evaluated Cross section Data used in Fast Neutron Methodology", RCN-73-083, Reactor Centrum Nederland, Petten (9/1973).

19. PAULSEN A. and WIDERA R., "$^{58}Ni(n,p)\ ^{58}Co$ and $^{54}Fe(n,p)\ ^{54}Mn$ Cross section Measurements for use as Thesholds Detector" in Chemical Nuclear data : Measurements and applications, M.L. BURRELL, Ed., Institutes of Civil Engineers, London (1971).

20. SIMONS R.L. and Mc ELROY W.N., "Evaluated reference cross-section Library" BNWL-1312, Batelle-Northwest laboratories (1970).